Available online at www.sciencedirect.com
ScienceDirect
International Journal of Non-Linear Mechanics 42 (2007) 118–131
INTERNATIONAL JOURNAL OF NON-LINEAR MECHANICS
www.elsevier.com/locate/nlm

Zener internal damping in modelling of axially moving viscoelastic beam with time-dependent tension

K. Marynowski, T. Kapitaniak*

Department of Dynamics, Technical University of Łódź, 90-924 Łódź, ul Stefanowskiego 1/15, Poland

Received 21 June 2006; received in revised form 8 August 2006; accepted 29 September 2006

Abstract

Non-linear vibrations of axially moving beam with time-dependent tension are investigated in this paper. The beam material is modelled as three-parameter Zener element. The Galerkin method and the fourth order Runge–Kutta method are used to solve the governing non-linear partial-differential equation. The effects of the transport speed, the tension perturbation amplitude and the internal damping on the dynamic behaviour of the system are numerically investigated. The Poincare maps and bifurcation diagrams are constructed to classify the vibrations. For small values of the transport speed and the amplitude of periodic perturbation the system is asymptotically stable with its response tending to zero. With the increase of parameters one can observe the coexistence of attractors. Regular and chaotic motion occur when the internal damping increases.

Keywords: Axially moving beam; Internal damping; Dynamic analysis

1. Introduction

Band saw blades, magnetic types, paper webs, fibber textiles, transmission cables are some technological examples of axially moving continua. Generally, the axially moving continuum in the form of thin, flat rectangular shape material with small flexural stiffness is called a web. Webs are moving at high speed, for example, in paper production the paper webs are transported with longitudinal speeds of up to 3000 m/min. Above the critical speed one can expect various dynamical instabilities mainly of divergent and flutter type. On the other hand, one important problem in these systems is the occurrence of large transverse vibrations due to tension variations termed as parametric vibrations. Dynamic response and the stability associated with parametric vibrations are of primary concern in the dynamic investigations of these systems. To ensure that the operating system is under stable working conditions, a full analysis of its dynamics has to be performed. Complete knowledge of the dynamical behaviour allows the prediction and control of instabilities.

Historically, one-dimensional string theory and beam theory were used in modelling the axially moving continua. For a review of the literature in this field up to the nineties of the previous century see papers by Wickert and Mote [1,2].

In recent years, much attention has been paid to non-linear dynamical behaviour, especially bifurcations and chaos in axially moving beam-like systems. Pelicano and Zirilli [3] analysed boundary layers and non-linear vibrations of an axially moving elastic beam with weak non-linearities and vanishing flexural stiffness. Ravindra and Zhu [4] investigated pitchfork-type bifurcation and chaos of axially accelerating beam in the supercritical region of transport speed. Chakraborty et al. [5] calculated non-linear complex modes of the axially moving beam by means of a combination method of a temporal harmonic balance and a spatial perturbation technique. Pelicano et al. [6,7] investigated bifurcations and parametric resonances of a moving beam. It is worth to note that they have verified their results by experimental measurements. Öz et al. [8] analysed vibrations of an axially accelerating beam by using

* Corresponding author. Tel.: +48 42 332231; fax: +48 42 365646.
E-mail address: tomaszka@p.lodz.pl (T. Kapitaniak).

0020-7462/$ - see front matter © 2007 Elsevier Ltd. All rights reserved.
doi:10.1016/j.ijnonlinmec.2006.09.006

Nomenclature

A	cross-section area of the beam	s	dimensionless axial transport speed
b	width of the beam	t	time
c	axial transport speed	w	transverse displacement of the beam
c_f	wave velocity	x, y	Cartesian co-ordinates
E	Young modulus of the beam material	z	dimensionless transverse displacement of the beam
$g_1, \ldots, g_7$	dimensionless coefficients	α	dimensionless amplitude of axial force
h	thickness of the beam	ε	strain component in x direction
J	inertia moment of the beam cross section	η	internal damping coefficient
l	length of the beam	v	dimensionless displacement of the beam centre
M	bending moment	ρ	mass density of the beam
N	perturbed axial stress	σ	stress component in x direction
P	tension force	Ω	frequency of periodic perturbation

the direct method of multiple scale. In [9] Pelicano and Vestroni numerically studied bifurcations and chaos in moving beam with transverse load.

The other important problem one can meet in considering the axially moving web is how to model the web material. In the above research on non-linear problems the axially moving materials were assumed to be elastic. The damping effects were neglected or modelled as a simple viscous damping [2]. However, paper webs, new plastics and composite materials webs, which are used in industry, need more realistic rheological models. Fung et al. [10] seems to be the first discussing the transverse non-linear free vibrations of an axially moving viscoelastic string subjected to constant initial stress. Zhang and Zu [11,12] investigated non-linear free and forced vibrations of parametrically excited moving viscoelastic belts. Dynamic stability of an axially moving beam-type system with uniform initial tension have been investigated by using two different rheologic models: two-parameters Kelvin–Voigt and four-parameters Burgers models in our paper [14]. The regular and chaotic vibrations of an axially moving viscoelastic beam subjected to tension variation were studied numerically in [15]. Recently, Yang and Chen [16] investigated bifurcations and chaos of an accelerating viscoelastic beam with geometric non-linearity. In this paper the viscoelastic beam material was constituted by one-dimensional Kelvin–Voigt rheologic model. Two-dimensional rheological element in modelling of axially moving viscoelastic web has been proposed by one of co-authors in 2006 [17].

The equations of motion of the axially moving viscoelastic beam with time-dependent tension have been derived in this paper. The three-parameter Zener rheological element has been used to model the beam material. From the partial-differential equation that governs the transverse vibrations of the system the fourth-order Galerkin truncated system is determined. The effects of the transport speed, the tension perturbation amplitude and the internal damping on the dynamic behaviour of the system were numerically investigated. The Poincare maps and bifurcation diagrams were constructed to classify the vibrations.

The paper is organized as follows. In Section 2 basing on the beam theory, we derive the equations of motion of the axially moving beam with three-parameter Zener rheological model of internal damping. In Section 2 we give full mathematical model of the axially moving beam as well. In Section 3 we discuss the results of our numerical investigations. The conclusions are presented in Section 4.

2. Equations of motion

A viscoelastic axially moving beam of the length l is considered. The beam moves at axial velocity c. The geometry of the system and the co-ordinates are shown in Fig. 1.

The problem of transverse oscillations of the axially moving continua in a state of uniform initial stress was investigated [13]. The results of the earlier studies give the following equation of motion in the y direction:

$$\rho A(-w_{,tt} - 2cw_{,xt} - c^2 w_{,xx}) + M_{,xx} + (Nw_{,x})_{,x} = 0. \tag{1}$$

The non-linear strain component in x direction is related to the displacement w by

$$\varepsilon(x,t) = \tfrac{1}{2} w_{,x}^2(x,t). \tag{2}$$

The tension P is characterized as a periodic perturbation on the steady-state tension

$$P = P_0 + P_1 \cos(\Omega t), \tag{3}$$

where P_0 is the initial axial force and P_1 the amplitude of axial force.

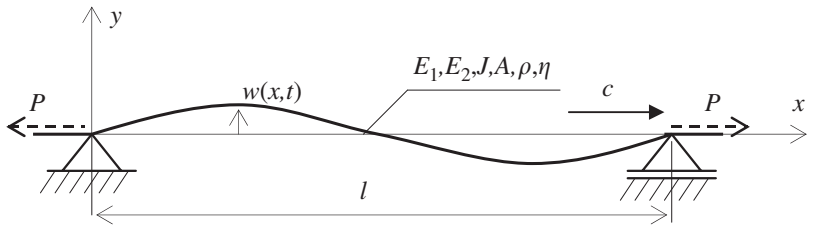

Fig. 1. Axially moving beam.

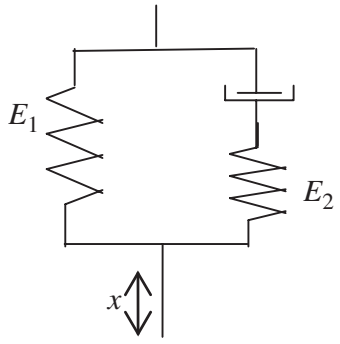

Fig. 2. Zener rheologic model.

The one-dimensional constitutive equation of a differential-type material obeys the relation

$$\Gamma_\sigma = \Xi\varepsilon, \tag{4}$$

where Γ and Ξ are differential operators defined as

$$\Gamma = \sum_{j=0}^{n} a_j \frac{\mathrm{d}^j}{\mathrm{d}t^j}, \quad \Xi = \sum_{j=0}^{m} b_j \frac{\mathrm{d}^j}{\mathrm{d}t^j}. \tag{5}$$

The model of internal damping introduced by Zener is shown in Fig. 2. For this three-parameter viscoelastic model of material the differential constitutive equation is

$$a_1\sigma_t + a_0\sigma = b_1\varepsilon_t + b_0\varepsilon, \tag{6}$$

where

$$a_1 = \eta,\ a_0 = E_2,\ b_1 = (E_1 + E_2)\eta,\ b_0 = E_1E_2. \tag{7}$$

The bending moment M is given

$$M = -(E_1 + E_2)Jw_{,xx} - J\eta w_{,xxt}. \tag{8}$$

where E_1, E_2 is the Young modules of the Zener model (Fig. 2).

Taking into account Eq. (8) the governing Eq. (1) has the following form:

$$w_{,tt} + 2cw_{,xt} + c^2w_{,xx} + \frac{J(E_1 + E_2)}{\rho A}w_{,xxxx} + \frac{J\eta}{\rho A}w_{,xxxxt} - \frac{1}{\rho A}(Nw_{,x})_{,x} = 0. \tag{9}$$

To obtain mathematical description of the viscoelastic beam model one should multiply Eq. (9) with operator Γ. Using Eqs. (2) and (3) and taking into account the dimensionless parameters

$$z = \frac{w}{h}, \quad \xi = \frac{x}{l}, \quad s = \frac{c}{c_f} = c\sqrt{\frac{A_\rho}{P_0}}, \quad \tau = t\frac{c_f}{l} = \frac{t}{l}\sqrt{\frac{P_0}{A_\rho}}, \quad \omega = \Omega l\sqrt{\frac{A\rho}{P_0}}, \quad c_f = \sqrt{\frac{P_0}{A\rho}}, \tag{10}$$

one receives

$$\begin{aligned} &z_{,\tau\tau\tau} + 3sz_{,\xi\tau\tau} + (3s^2 - 1 - \alpha\cos(\omega\tau))z_{,\xi\xi\tau} + (s^2 - 1 - \alpha\cos(\omega\tau))sz_{,\xi\xi\xi} + g_1z_{,\tau\tau} + 2g_1sz_{,\xi\tau} + g_1(s^2 - 1 - \alpha\cos(\omega\tau))z_{,\xi\xi} \\ &\quad + g_2z_{,\xi\xi\xi\xi} + g_3z_{,\xi\xi\xi\xi\tau} + g_4z_{,\xi\xi\xi\xi\xi} + g_5z_{,\xi\xi\xi\xi\tau\tau} + g_5sz_{,\xi\xi\xi\xi\xi\tau} - \frac{3}{2}g_6z_{,\xi}^2z_{,\xi\xi} - g_7s(2z_{,\xi\xi}^2z_{,\xi} + z_{,\xi}^2z_{,\xi\xi\xi}) \\ &\quad - g_7(2z_{,\xi}z_{,\xi\tau}z_{,\xi\xi} + z_{,\xi}^2z_{,\xi\xi\tau}) = 0, \end{aligned} \tag{11}$$

where

$$g_1 = \frac{E_2 l}{\eta c_f}, \quad g_2 = \frac{(E_1 + E_2) J E_2}{\rho A \eta l c_f^3}, \quad g_3 = \frac{(E_1 + E_2) J}{\rho A l^2 c_f^2} + \frac{E_2 J}{\rho A l^2 c_f^2}, \quad \alpha = \frac{P_1}{P_0},$$
$$g_4 = \frac{(E_1 + E_2) J}{\rho A l^2 c_f^2}, \quad g_5 = \frac{J \eta}{\rho A l^3 c_f}, \quad g_6 = \frac{E_1 E_2 h^2}{\rho \eta l c_f^3}, \quad g_7 = \frac{(E_1 + E_2) h^2}{\rho l^2 c_f^2}. \tag{12}$$

The boundary conditions

$$z(0, \tau) = z(1, \tau) = 0, \quad z_{,\xi\xi}(0, \tau) = z_{,\xi\xi}(1, \tau) = 0. \tag{13}$$

The problems represented by Eq. (11) together with boundary conditions (13) have been solved using the Galerkin method. The following finite series representation of the dimensionless transverse displacement has been assumed

$$z(\xi, \tau) = \sum_{i=1}^{n} \sin(i \pi \xi) q_i(\tau), \tag{14}$$

where $q_i(\tau)$ is the generalized displacement.

The four-term finite series representation of the dimensionless transverse displacement of the beam has been taken in numerical investigations. The even order truncations are receivable because the gyroscopic coupling in the mathematical model is taken into consideration. Substituting Eq. (14) into Eq. (11) and using the orthogonality condition one determines the set of ordinary differential equations. For $n = 4$ the equations are shown in the Appendix (Eq. A.1). To analyse the dynamic behaviour of the considered system the set of ordinary differential equations has been integrated.

3. Numerical results

Poincare maps and bifurcation diagrams are modern techniques used to analyse non-linear systems. These maps are the convenient tools to identify the dynamic behaviour especially chaos. In bifurcations diagrams dynamical behaviour may be viewed globally over a range of parameters values and compared simultaneously with various types of motions.

In this paper the Poincare maps and bifurcation diagrams have been determined for the non-dimensional displacement of the centre of the moving beam in the following form:

$$v(\tfrac{1}{2}, iT) = q_1(iT) - q_3(iT), \tag{15}$$

where $T = 2\pi/\omega$, $i = 1, 2, 3, \ldots$.

Numerical investigations have been carried out for the beam model of the steel web. Parameters data: length $l = 1$ m, width $b = 0.2$ m, thickness $h = 0.0015$ m, mass density $\rho = 7800\,\mathrm{kg/m^3}$, Young's modulus along x: $E_x = 0.2 \times 10^{12}\,\mathrm{N/m^2}$, initial stress $N_0 = 2500\,\mathrm{N/m}$. It is worth to note that in the previous investigations with two-parameter Kelvin–Voigt and four-parameter Burgers rheological models of material the same numerical data of the steel web have been taken into account [14,15].

The fourth-order Runge–Kutta method was used to integrate ordinary differential equations and analyse the dynamic behaviour of the system. The bifurcation diagrams are presented by varying the dimensionless parameters: transport speed s, amplitude of the tension periodic perturbation α, and the internal damping coefficient g_5, while the dimensionless frequency of the periodic perturbation ω and the non-dimensional stiffness of the beam g_4 are kept constant at $\omega = 1$ and $g_4 = 0.025$, respectively. At each set of parameters the first 2000 points of the Poincare map have been discarded in order to exclude the transient vibration and the displacement of the next 100 points have been plotted on the bifurcation diagrams.

3.1. Linearized system

The stability and instability regions of the linearized system (A.1) in the form of the stability boundaries map in the internal damping–transport speed area are shown in Fig. 3. The boundaries have been calculated for three amplitude values of the tension periodic perturbation ($\alpha = 0$, 0.25, 0.5). The analysis of the linearized system predicts exponentially growing oscillations in supercritical region of transport speed. The critical value of the transport speed increases with the increase of damping coefficient g_5.

3.2. Non-linear system

At first, the parametrically unexcited non-linear system was investigated ($\alpha = 0$). To show the dynamic behaviour of the beam the bifurcation diagram of the dimensionless displacement v given by Eq. (15), the Poincare maps, the phase portrait and time history for $g_5 = 1.778 \times 10^{-4}$ are presented in Figs. 4, 5 and 6, respectively. The dimensionless transport speed s has been used as the

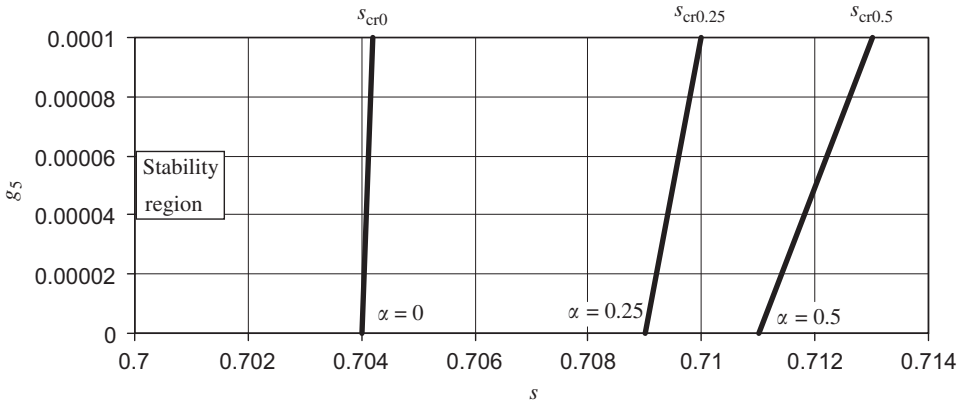

Fig. 3. Stability boundaries of the linearized system (A.1).

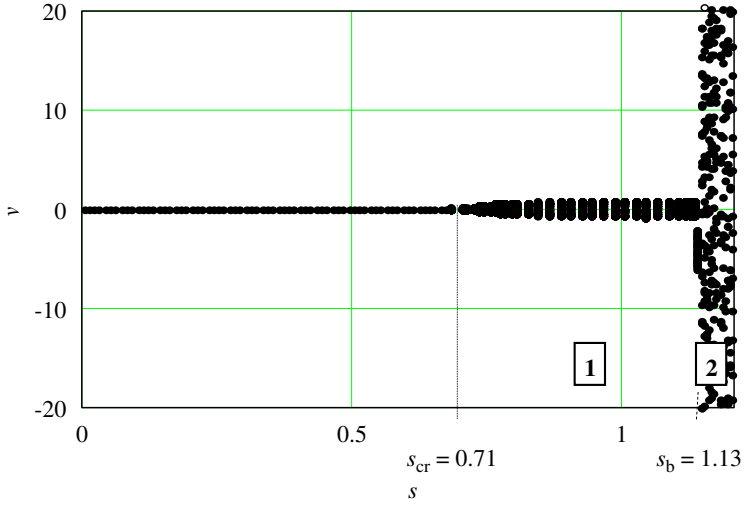

Fig. 4. Bifurcation diagram: $g_5 = 1.778 \times 10^{-4}$, $\omega_0 = 3.5$, $\alpha = 0$.

bifurcation parameter. To obtain the Poincare maps in this parametrically unexcited case the dimensionless fundamental natural frequency $\omega_0 = 3.5$ has been taken into consideration. In Fig. 4 one can observe supercritical Hopf-type bifurcation at the transport speed $s = s_{cr} = 0.71$. It is worth to note that in the previous case of the Burger rheological model of the beam material, the transport speed $s = 0.7$ has been identified as the critical transport speed for the considered damping coefficient value [14].

Though the analysis of the linearized system predicts exponentially growing oscillations for $s > s_{cr}$, non-linear damped oscillations which tend to the stable limit cycle motion occur (region 1 in Fig. 4). The Poincare map in Fig. 5a and the phase portrait and time history in Fig. 6 show the dynamic behaviour of the non-linear system in this region of transport speed for the initial conditions close to zero.

If the transport speed is increased further at $s_b = 1.13$ the second bifurcation occurs. At the transport speeds above the bifurcation point (region 2 in Fig. 4), the parametrically unexcited non-linear system exhibits global motion between two centre points. The Poincare map in Fig. 4 and the phase portrait in Fig. 7 show the dynamic behaviour of the non-linear system in this region of transport speed It is worth to note that in the previous case of the Kelvin–Voigt rheological model of the beam material, the transport speed $s = 1.12$ has been identified as the critical transport velocity when the pitchfork-type bifurcation occurs [15]. In the considered case of Zener rheological model above this transport speed one can observe the coexistence of attractors.

Next, the non-linear parametrically excited system was investigated. The bifurcations diagram of the dimensionless displacement v versus the dimensionless transport speed s for the specific amplitude value of the tension periodic perturbation $\alpha = 0.25$ and the internal damping coefficient $g_5 = 1.778 \times 10^{-4}$ is shown in Fig. 8. In this case, the system is asymptotically stable with its response tending to zero for $s < 0.71$. At the transport speed $s = 0.71$ the zero critical point loses its stability and quasi-periodic motion occurs. Fig. 9 shows the Poincare map of the system behaviour in this region of transport speed. If the transport speed is increased further ($s = 0.85$) the second Hopf bifurcation occurs and chaotic motion appears (Fig. 10). As a result of the Hopf bifurcation we can observe that regular tori (Fig. 9) becomes a strange attractor of fractal structure. At $s = 1.05$ the inverse Hopf bifurcation can be observed and the period-2 motion occurs in the region $s = 1.05 \div 1.12$. Then two points represent two periodic orbits in bifurcation diagram. At $s = 1.12$ the explosive bifurcation occurs and the large quasi-periodic motion appears.

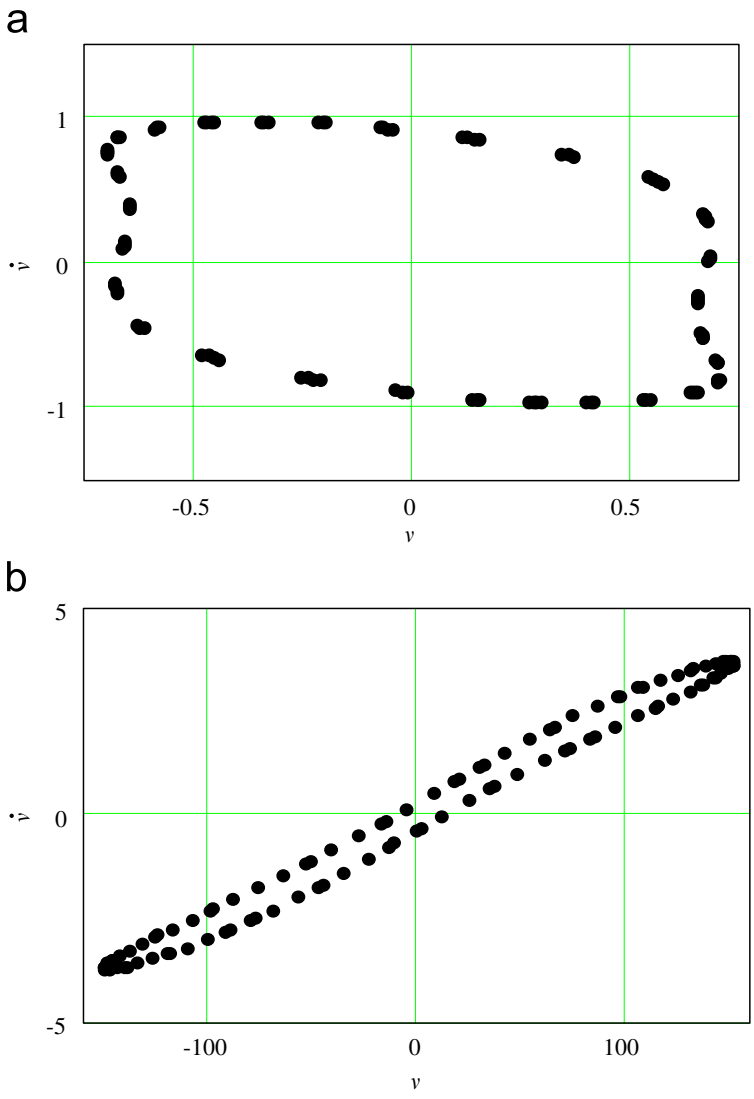

Fig. 5. The Poincare maps: $g_5 = 1.778 \times 10^{-4}$, $\alpha = 0$, $\omega_0 = 3.5$; (a) $s = 1.0$; (b) $s = 1.25$.

The bifurcations diagram of the displacement v versus the transport speed s for larger value of parametric excitation $\alpha = 0.5$ is shown in Fig. 11. In this case at $s = 0.72$ the equilibrium loses its stability and quasi-periodic motion occurs. Fig. 12 shows the phase portrait and time history of the non-linear system motion in this region of transport speed for the initial conditions close to zero. At the supercritical transport speeds periodic motion regions are interrupted by short chaotic motion until at $s = 1.15$ explosive bifurcation occurs and the chaotic motion appears (Fig. 11).

The bifurcation plot of the dimensionless displacement v given by Eq. (15) against the non-dimensional internal damping coefficient g_5 for $\alpha = 0.25$ and various axial speeds $s = 0.75$, 0.875 and 1.0 are shown in Figs. 13, 14 and 15, respectively. At $s = 0.75$ for small values of internal damping ($g_5 < 1.1 \times 10^{-3}$) the quasi-periodic motion occurs (previous Fig. 9 shows the Poincare map of the system behaviour in this region). With the increase of internal damping at $g_5 = 1.1 \times 10^{-3}$ the inverse Hopf-type bifurcation occurs and finally the system is asymptotically stable with its response tending to zero (Fig. 13).

With the increase of the dimensionless transport speed at $s = 0.875$ the quasi-periodic region is interrupted by periodic motion (Fig. 14). At $s = 1.0$ for small values of internal damping ($g_5 < 1.1 \times 10^{-3}$) the period-2 motion appears and next for larger values of the dimensionless internal damping coefficient, the quasi-periodic and chaotic motion occur. The Poincare map in Fig. 16 shows the strange attractor created in the bifurcation which takes places at the internal damping $g_5 = 3.804 \times 10^{-3}$. Then the small quasi-periodic attractor presented in Fig. 9 transforms in larger attractor shown in Fig. 17.

Next the dimensionless amplitude of the tension periodic perturbation α has been used as the bifurcation parameter. For small values of these bifurcation parameter and small values of transport speed the system is stable with its response tending to zero. The bifurcation diagram in Fig. 18 shows the Poincare maps of the dimensionless displacement v against the perturbation amplitude α for greater transport speed value $s = 0.75$ and $g_5 = 1.778 \times 10^{-4}$. For lower α values ($\alpha < 0.62$) the quasi-periodic motion occurs.

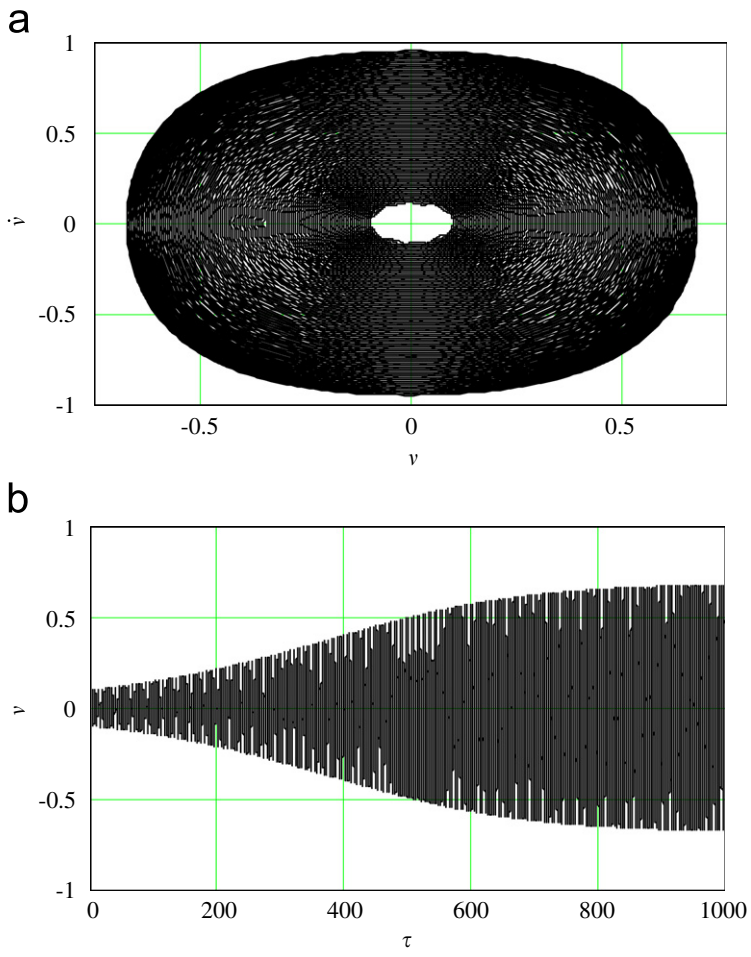

Fig. 6. The phase portrait (a) and time history (b) of the solution of (A.1): $s = 1$, $g_5 = 1.778 \times 10^{-4}$, $\alpha = 0$.

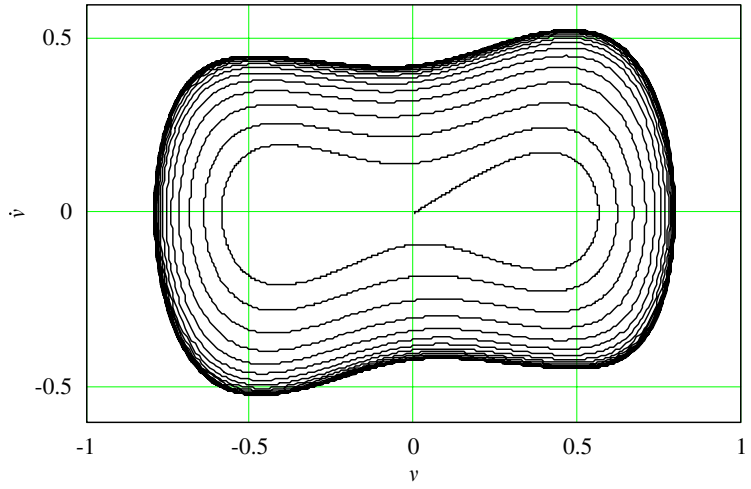

Fig. 7. The phase portrait of the solution of (A.1): $s = 1.15$, $g_5 = 10^{-3}$, $\alpha = 0$, $\omega_0 = 3.5$.

Previous Fig. 9 shows the Poincare map of the system behaviour in this region of the tension amplitude value. With the increase of the tension at $\alpha = 0.62$ the quasi-periodic attractor bifurcates into the period-6 attractor, at $\alpha = 0.78$ into the period-4 attractor and finally at $\alpha = 0.8$ into the period-2 attractor (Fig. 18). For greater axial velocity $s = 1.0$ the bifurcation diagram in Fig. 19 and the Poincare maps in Figs. 20 and 21 show the quasi-periodic and chaotic motions of the axially moving viscoelastic beam.

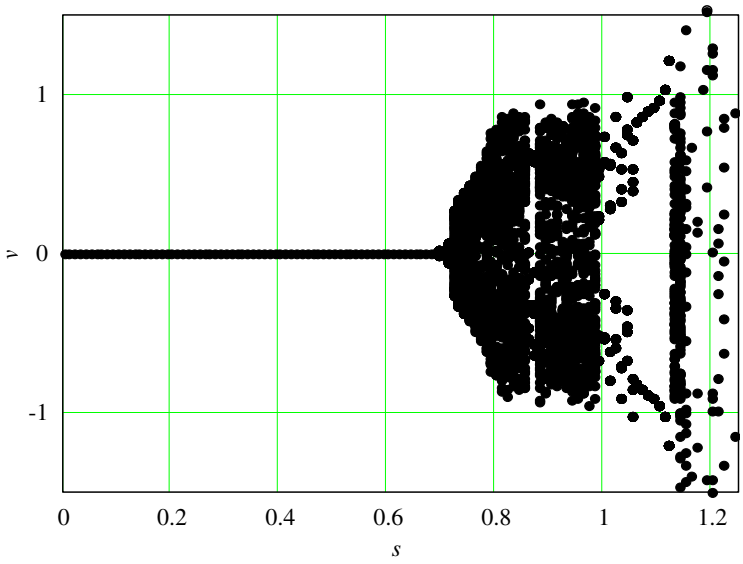

Fig. 8. Bifurcation diagram of the non-linear system (A.1) for $g_5 = 1.778 \times 10^{-4}$, $\alpha = 0.25$.

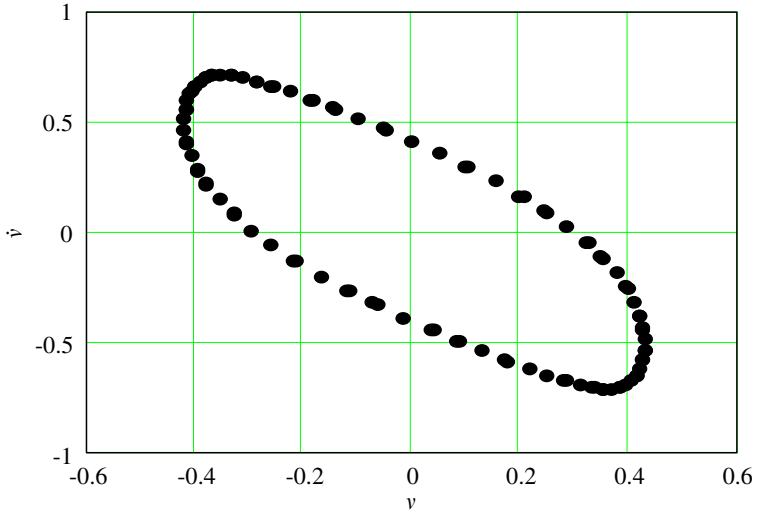

Fig. 9. The Poincare map: $g_5 = 1.778 \times 10^{-4}$, $\alpha = 0.25$, $s = 0.75$.

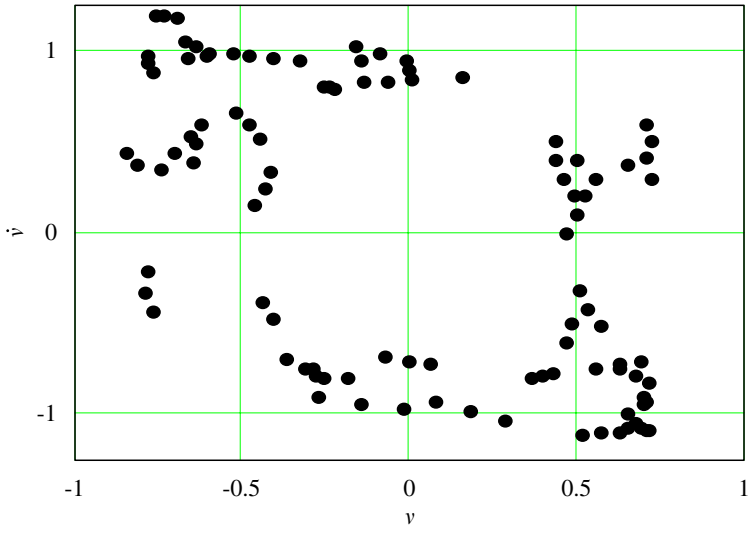

Fig. 10. The Poincare map: $g_5 = 1.778 \times 10^{-4}$, $\alpha = 0.25$, $s = 0.93$.

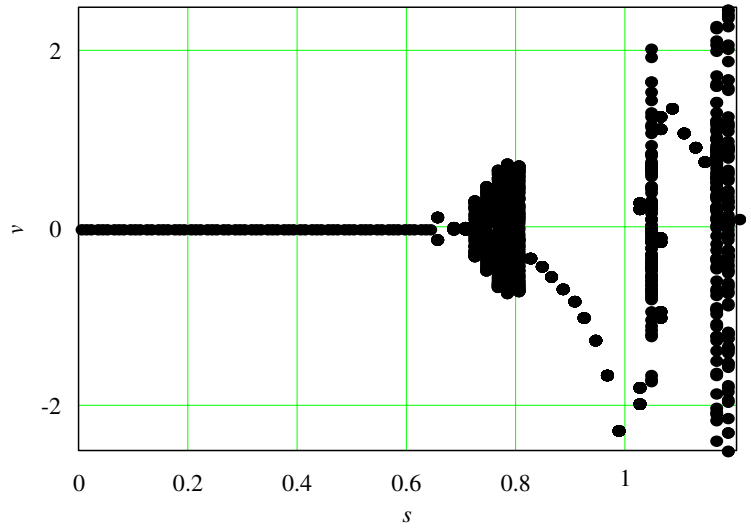

Fig. 11. Bifurcation diagram of the non-linear system (A.1) for $g_5 = 1.778 \times 10^{-4}$, $\alpha = 0.5$.

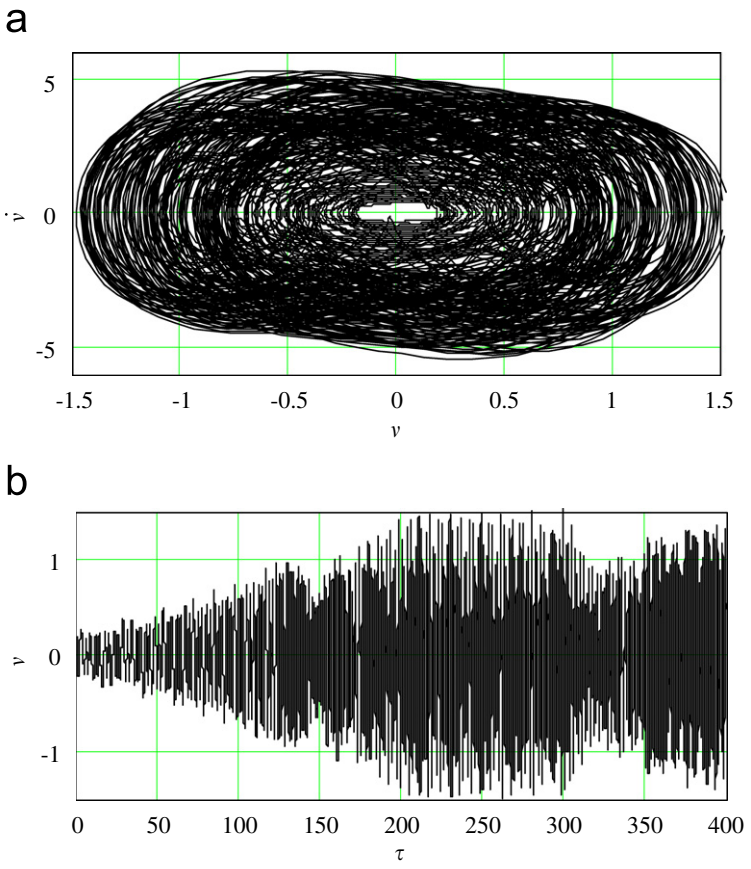

Fig. 12. The phase portrait (a) and the time history (b) of the solution of the non-linear system (A.1): $s = 0.76$, $\alpha = 0.5$, $g_5 = 1.778 \times 10^{-4}$.

4. Conclusions

The dynamic investigations of the axially moving viscoelastic beam with time-dependent tension are carried out in this paper. The beam model material as the Zener reological element is considered. The general form of the differential equation of transverse oscillations of the considered system is derived together with the differential constitutive low for the rheological model. The Galerkin

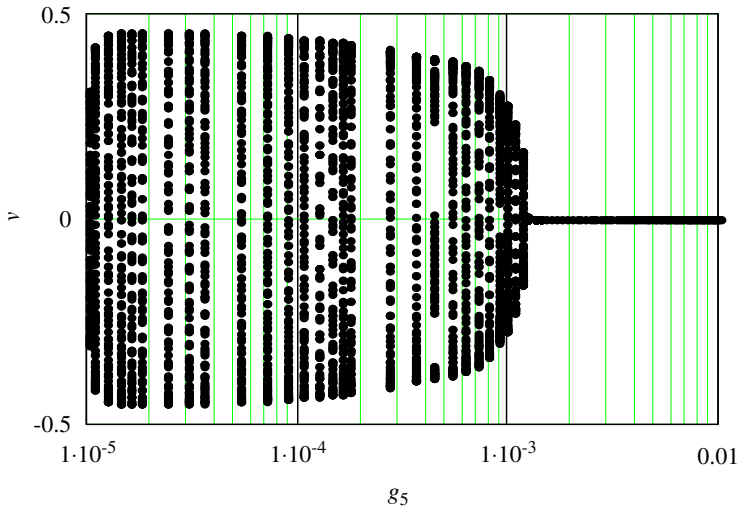

Fig. 13. Bifurcation diagram of the non-linear system (A.1) for $s = 0.75$, $\alpha = 0.25$.

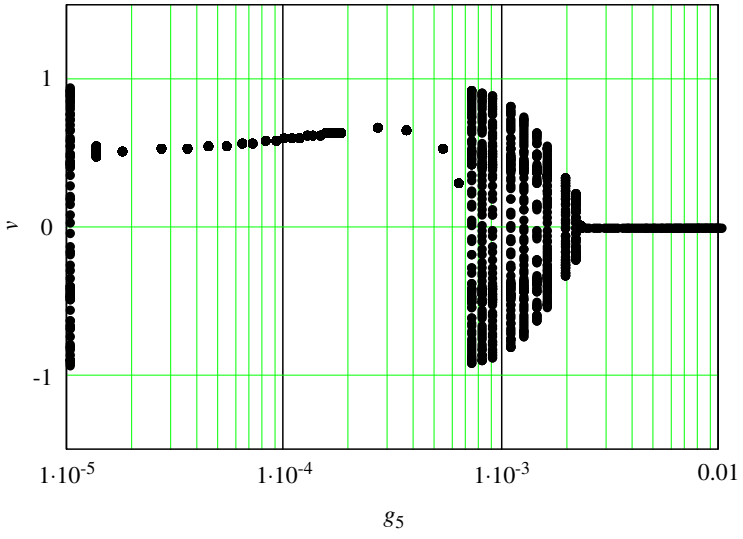

Fig. 14. Bifurcation diagram of the non-linear system (A.1) for $s = 0.875$, $\alpha = 0.25$.

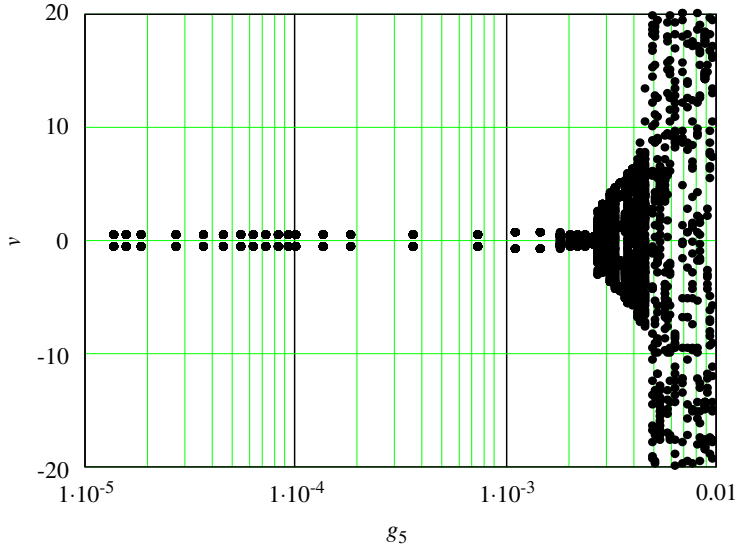

Fig. 15. Bifurcation diagram of the non-linear system (A.1) for $s = 1.0$, $\alpha = 0.25$.

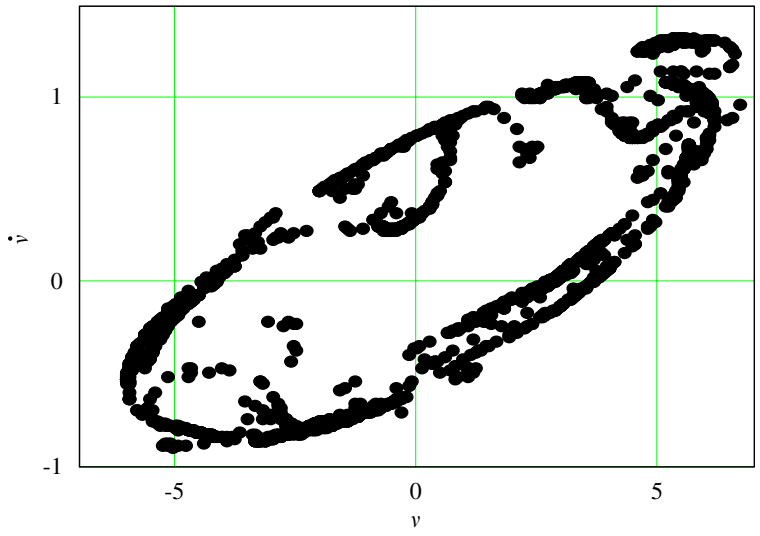

Fig. 16. The Poincare map: $s = 1.0$, $\alpha = 0.25$, $g_5 = 3.804 \times 10^{-3}$.

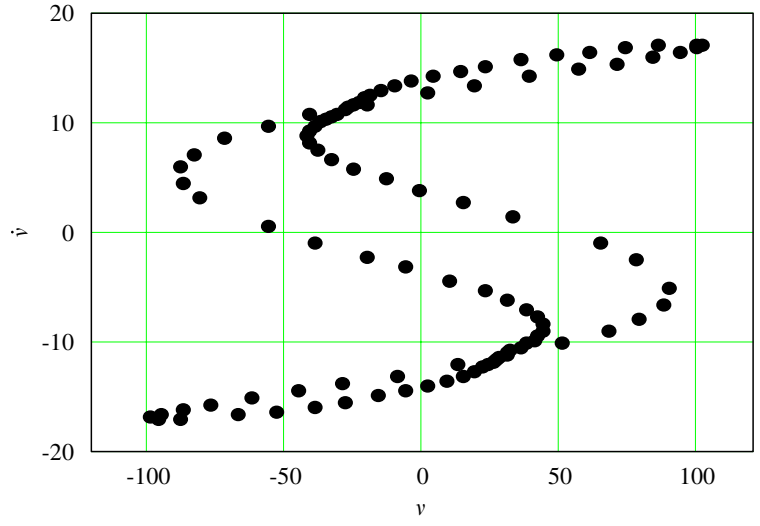

Fig. 17. The Poincare map: $s = 1.0$, $\alpha = 0.25$, $g_5 = 7.111 \times 10^{-3}$.

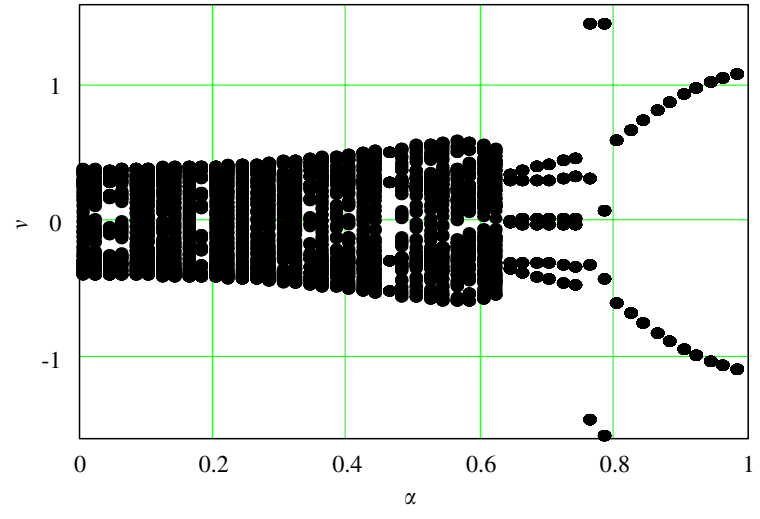

Fig. 18. Bifurcation diagram of the non-linear system (A.1) for $s = 0.75$, $g_5 = 1.778 \times 10^{-4}$.

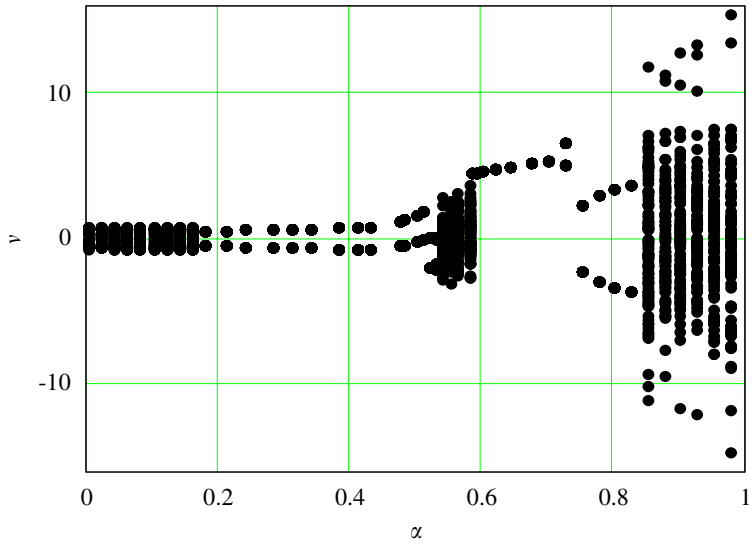

Fig. 19. Bifurcation diagram of the non-linear system (A.1) for $s = 1$, $g_5 = 1.778 \times 10^{-4}$.

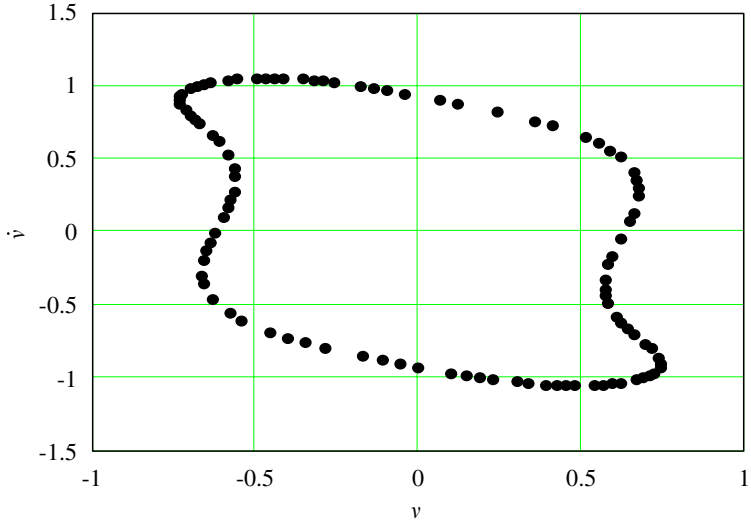

Fig. 20. The Poincare map: $s = 1.0$, $\alpha = 0.1$, $g_5 = 1.778 \times 10^{-4}$.

method is applied to simplify the governing non-linear partial-differential equation into fourth-order truncated system defined by the set of ordinary differential equations.

The fourth-order Runge–Kutta method was used to integrate ordinary differential equations and analyse the dynamic behaviour of the system. The Poincare maps have been constructed to classify the vibrations. The bifurcations diagrams are obtained by varying the transport speed, the amplitude of the tension periodic perturbation and the internal damping coefficient, while the frequency of the periodic perturbation and the stiffness of the beam are kept constant.

The numerical investigations have been carried out for the beam model of the steal web. The same numerical data of the web have been taken into consideration like in the previous investigations with two-parameter Kelvin–Voigt and four-parameter Burgers rheological models of material. The critical transport speed of the non-linear, parametrically excited viscoelastic beam with the Zener model of material is equal to the one with the Burgers model of material and significantly smaller than the one with the Kelvin–Voigt model.

In the case when the transport speed was taken as the bifurcation parameter the system is asymptotically stable with its response tending to zero for $s < 0.71$. At the transport speed $s = 0.71$ the zero critical point loses its stability and quasi-periodic motion occurs. For greater axial velocity the quasi-periodic, periodic and chaotic motions occurs. The axial transport speed, when the explosive bifurcation of investigated system occurs, is equal to the critical transport velocity of the previous model with the Kelvin–Voigt rheological model of the beam material, when the pitchfork-type bifurcation occurs.

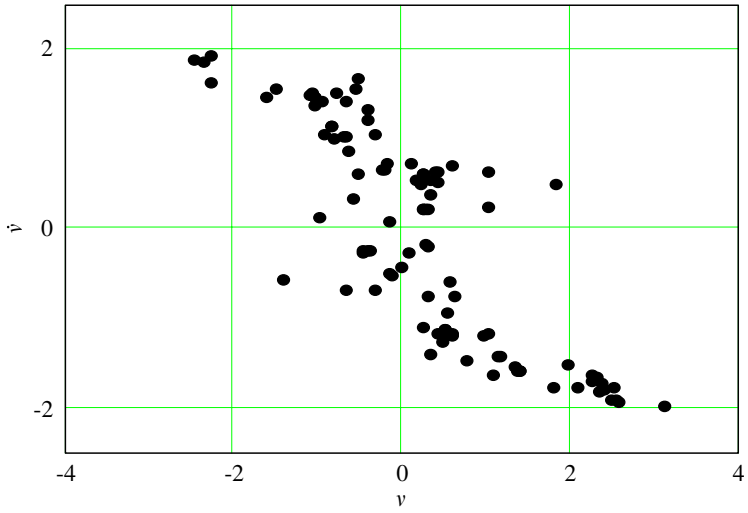

Fig. 21. The Poincare map: $s = 1.0$, $\alpha = 0.56$, $g_5 = 1.778 \times 10^{-4}$.

When the internal damping coefficient is taken as the bifurcation parameter for small values of internal damping the quasi-periodic motion occurs. With the increase of the transport speed in this region of the internal damping, the quasi-periodic region is interrupted by periodic motion. When the transport speed increases at first the small quasi-periodic attractor transforms into larger quasi-periodic attractor and finally into the chaotic attractor.

When the amplitude of periodic perturbation has been taken as the bifurcation parameter one can observe the dynamic behaviour typical for non-linear systems which are determined in multi-dimensional phase space. For small values of these bifurcation parameter and small values of the transport speed the system is stable with its response tending to zero. With the increase of the bifurcation parameters the chaotic motion and regular motion alternately appear. It means that the appearance of the hiperchaotic attractor is possible in these ranges of bifurcation parameters.

Appendix A

The set of ordinary differential equations of the viscoelastic beam model with the Zener model of material ($n = 4$):

$$
\begin{aligned}
\ddot{q}_1 = & -(g_1 + g_5\pi^4)\ddot{q}_1 + 8s\ddot{q}_2 + ((3s^2 - 1 - \alpha\cos(\omega\tau))\pi^2 - g_3\pi^4)\dot{q}_1 + ((16/3)g_1 + (128/3)g_5\pi^4)s\dot{q}_2 \\
& + (g_1(s^2 - 1 - \alpha\cos(\omega\tau))\pi^2 - g_2\pi^4)q_1 + (-(32/3)\pi^2 s(s^2 - 1 - \alpha\cos(\omega\tau)) + (128/3)g_5\pi^4 s)q_2 \\
& + (-(256/15)\pi^2 s(s^2 - 1 - \alpha\cos(\omega\tau)) + (4096/15)g_4\pi^4 s)q_4 + ((32/15)g_1 s + (4096/15)g_5\pi^4 s)\dot{q}_4 + (16/5)s\ddot{q}_4 \\
& -3g_6\pi^4((1/8)q_1^3 + q_1q_2^2 + (9/4)q_1q_3^2 + (3/8)q_1^2q_3 + (3/2)q_2^2q_3 + 2q_1q_2q_4 + 4q_1q_4^2 + 6q_2q_3q_4) - 2g_7\pi^4((3/8)q_1^2\dot{q}_1 \\
& + (3/8)q_1^2\dot{q}_3 + (3/4)q_1q_3\dot{q}_1 + (3/2)q_2^2\dot{q}_3 + 3q_2q_3\dot{q}_2 + 2q_1q_2\dot{q}_2 + q_2^2\dot{q}_1 + (9/4)q_3^2\dot{q}_1 + (9/2)q_1q_3\dot{q}_3 + 2q_1q_4\dot{q}_2 \\
& + 2q_1q_2\dot{q}_4 + 2q_2q_4\dot{q}_1 + 6q_2q_4\dot{q}_3 + 6q_2q_3\dot{q}_4 + 6q_3q_4\dot{q}_2 + 8q_1q_4\dot{q}_4 + 4q_4^2\dot{q}_1) + 2g_7\pi^4((144/7)\,q_1q_2q_3 \\
& + (7936/315)q_2^2q_4 + (20086528/266805)q_2q_4^2 + (4432/55)q_3^2q_4 + (96256/2145)q_4^3).
\end{aligned}
$$

$$
\begin{aligned}
\ddot{q}_2 = & -8s\ddot{q}_1 - (g_1 + 16g_5\pi^4)\ddot{q}_2 + (72/5)s\ddot{q}_3 - ((16/3)g_1 + (8/3)g_5\pi^4)s\dot{q}_1 + (4(3s^2 - 1 - \alpha\cos(\omega\tau))\pi^2 - 16g_3\pi^4)\dot{q}_2 \\
& + ((48/5)g_1 + (1944/5)g_5\pi^4)s\dot{q}_3 + ((8/3)\pi^2(s^2 - 1 - \alpha\cos(\omega\tau)) - (8/3)g_4\pi^4)sq_1 + (4g_1\pi^2(s^2 - 1 - \alpha\cos(\omega\tau)) \\
& - 16g_2\pi^4)q_2 + ((1944/5)g_4\pi^4 - (216/5)\pi^2(s^2 - 1 - \alpha\cos(\omega\tau)))sq_3 - 3g_6\pi^4(q_1^2q_2 + 2q_2^3 + 9q_2q_3^2 + 3q_1q_2q_3 \\
& + q_1^2q_4 + 6q_1q_3q_4 + 16q_4^2q_2 + 9q_3^2q_4) - 2g_7\pi^4(3q_1q_2\dot{q}_3 + 3q_1q_3\dot{q}_2 + 6q_2^2\dot{q}_2 + 2q_1q_4\dot{q}_1 + q_1^2\dot{q}_4 + 3q_2q_3\dot{q}_1 \\
& + 2q_1q_2\dot{q}_1 + 18q_2q_3\dot{q}_3 + q_1^2\dot{q}_2 + 9q_3^2\dot{q}_2 + 6q_1q_4\dot{q}_3 + 6q_1q_3\dot{q}_4 + 6q_3q_4\dot{q}_1 + 18q_3q_4\dot{q}_3 + 9q_3^2\dot{q}_4 \\
& + 16q_4^2\dot{q}_2 + 32q_2q_4\dot{q}_4) + 2g_7\pi^4 s((4/15)q_1^3 + (22356/385)q_3^3 + (784/15)q_2^2q_3 + (976/105)q_1q_2^2 + (508/35)q_1q_3^2 \\
& + (468/35)q_1^2q_3 + (3776/63)q_1q_2q_4 + (81728/3465)q_1q_4^2 + (107712/605)q_2q_3q_4 + (1219616/4095)q_3q_4^2).
\end{aligned}
$$

$$\begin{aligned}
\dddot{q}_3 = {} & (-g_1 + 81g_5\pi^4)\ddot{q}_3 - (72/5)s\ddot{q}_2 + (9(3s^2 - 1 - \alpha\cos(\omega\tau))\pi^2 - 81g_3\pi^4)\dot{q}_3 - ((48/5)g_1 + (384/5)g_5\pi^4)s\dot{q}_2 \\
& + (9g_1(s^2 - 1 - \alpha\cos(\omega\tau))\pi^2 - 81g_2\pi^4)q_3 + ((96/5)\pi^2 s(s^2 - 1 - \alpha\cos(\omega\tau)) - (384/5)g_5\pi^4 s)q_2 \\
& + (-(768/7)\pi^2 s(s^2 - 1 - \alpha\cos(\omega\tau)) + (12288/7)g_4\pi^4 s)q_4 + ((96/7)g_1 s + (12288/7)g_5\pi^4 s)\dot{q}_4 + (144/7)s\ddot{q}_4 \\
& - 3g_6\pi^4((81/8)q_3^3 + (1/8)q_1^3 + (9/4)q_1^2 q_3 + 6q_1 q_2 q_4 + (3/2)q_1 q_2^2 + 18q_2 q_3 q_4 + 36q_3 q_4^2 + 9q_2^2 q_3) \\
& -2g_7\pi^4((9/2)q_1 q_3\dot{q}_1 + 6q_1 q_4\dot{q}_2 + (3/8)q_1^2\dot{q}_1 + 3q_1 q_2\dot{q}_2 + (9/4)q_1^2\dot{q}_3 + 6q_2 q_4\dot{q}_1 + 6q_1 q_2\dot{q}_4 + 18q_2 q_3\dot{q}_2 + (3/2)q_2^2\dot{q}_1 \\
& + 36q_4^2\dot{q}_3 + 18q_2 q_4\dot{q}_3 + 18q_2 q_3\dot{q}_4 + 18q_3 q_4\dot{q}_2 + 72q_3 q_4\dot{q}_4 + 9q_2^2\dot{q}_3 + (243/8)q_3^2\dot{q}_3) + 2g_7\pi^4 s(-(192/45)q_2^3 \\
& + (72/35)q_1^2 q_2 + (79872/315)q_4^3 + (1072/35)q_1^2 q_4 + (5328/105)q_1 q_2 q_3 + (52992/385)q_2^2 q_4 + (2016/33)q_1 q_3 q_4 \\
& + (19224/385)q_2 q_3^2 + (119664/455)q_3^2 q_4 + (18176/455)q_2 q_4^2).
\end{aligned}$$

$$\begin{aligned}
\dddot{q}_4 = {} & -(16/5)s\ddot{q}_1 - (g_1 + 256g_5\pi^4)\ddot{q}_4 - (144/7)s\ddot{q}_3 - ((32/15)g_1 + (16/15)g_5\pi^4)s\dot{q}_1 + (16(3s^2 - 1 - \alpha\cos(\omega\tau))\pi^2 \\
& - 256g_3\pi^4)\dot{q}_4 - ((96/7)g_1 + (3888/7)g_5\pi^4)s\dot{q}_3 + ((16/15)\pi^2 s(s^2 - 1 - \alpha\cos(\omega\tau)) - (16/15)g_4\pi^4 s)q_1 \\
& + (16g_1\pi^2(s^2 - 1 - \alpha\cos(\omega\tau)) - 256g_2\pi^4)q_4 + (-(3888/7)g_4\pi^4 + (432/7)\pi^2(s^2 - 1 - \alpha\cos(\omega\tau)))sq_3 \\
& - 3g_6\pi^4(q_1^2 q_2 + 32q_4^3 + 9q_2 q_3^2 + 4q_1^2 q_4 + 6q_1 q_2 q_3 + 16q_2^2 q_4 + 9q_2 q_3^2 + 36q_3^2 q_4) - 2g_7\pi^4(6q_1 q_2\dot{q}_3 + 6q_1 q_3\dot{q}_2 \\
& + 9q_3^2\dot{q}_2 + 8q_1 q_4\dot{q}_1 + 4q_1^2\dot{q}_4 + 6q_2 q_3\dot{q}_1 + 2q_1 q_2\dot{q}_1 + 18q_2 q_3\dot{q}_3 + q_1^2\dot{q}_2 + 96q_4^2\dot{q}_4 + 32q_2 q_4\dot{q}_2 + 72q_3 q_4\dot{q}_3 \\
& + 16q_2^2\dot{q}_4 + 36q_3^2\dot{q}_4) + 2g_7\pi^4 s(-(104/105)q_1^3 - (21384/455)q_3^3 - (10656/385)q_2^2 q_3 + (3424/315)q_1 q_2^2 \\
& + (36792/495)q_1 q_3^2 + (88/105)q_1^2 q_3 + (24846976/266805)q_1 q_2 q_4 + (178304/2145)q_1 q_4^2 + (70016/273)q_2 q_3 q_4 \\
& + (36928/315)q_3 q_4^2). \qquad \text{(A.1)}
\end{aligned}$$

References

[1] J.A. Wickert, C.D. Mote Jr., Current research on the vibration and stability of axially moving materials, Shock Vib. Digest 20 (1988) 3–13.
[2] J.A. Wickert, C.D. Mote Jr., Classical vibration analysis of axially-moving continua, J. Appl. Mech. ASME 57 (1990) 738–744.
[3] F. Pelicano, F. Zirilli, Boundary layers and non-linear vibrations in an axially moving beam, Int. J. Non-Linear Mech. 33 (1997) 691–711.
[4] B. Ravindra, W.D. Zhu, Low dimensional chaotic response of axially accelerating continuum in the supercritical regime, Arch. Appl. Mech. 68 (1998) 195–205.
[5] G. Chakraborty, A.K. Mallik, H. Hatwal, Non-linear vibration of a travelling beam, Int. J. Non-linear Mech. 34 (1999) 655–670.
[6] F. Pelicano, F. Vestroni, Non-linear dynamics and bifurcations of an axially moving beam, ASME J. Vib. Acoust. 122 (2000) 21–30.
[7] F. Pelicano, A. Fregolent, A. Bertuzzi, F. Vestroni, Primary and parametric non-linear resonances of a power transmission belt, J. Sound Vib. 244 (2001) 669–684.
[8] H.R. Öz, M. Pakdemirli, H. Boyaci, Non-linear vibrations and stability of an axially moving beam with time-dependent velocity, Int. J. Non-linear Mech. 36 (2001) 107–115.
[9] F. Pelicano, F. Vestroni, Complex dynamics of high-speed axially moving systems, J. Sound Vib. 258 (2002) 31–44.
[10] R.-F. Fung, J.-S. Huang, Y.-C. Chen, Non-linear dynamic analysis of the viscoelastic string with a harmonically varying transport speed, Comput. Struct. 66 (6) (1998) 777–784.
[11] L. Zhang, J.-W. Zu, Non-linear vibrations of viscoelastic moving belts, part I and II, J. Sound Vib. 216 (1998) 75–105.
[12] L. Zhang, J.-W. Zu, Non-linear vibrations of parametrically excited viscoelastic moving belts part I and II, J. Appl. Mech. 66 (2) (1999) 396–409.
[13] K. Marynowski, Non-linear vibration of axially moving orthotropic web, Mech. Mech. Eng. 4 (2) (1999) 131–136.
[14] K. Marynowski, T. Kapitaniak, Kelvin–Voigt versus Burgers internal damping in modelling of axially moving viscoelastic web, Int. J. Non-linear Mech. 37 (7) (2002) 1147–1161.
[15] K. Marynowski, Non-linear vibrations of an axially moving viscoelastic web with time-dependent tension, Chaos Solitons Fractals 21 (2004) 481–490.
[16] X.-D. Yang, L.-Q. Chen, Bifurcation and chaos of an axially accelerating viscoelastic beam, Chaos Solitions Fractals 23 (2005) 249–258.
[17] K. Marynowski, Two-dimensional rheological element in modelling of axially moving viscoelastic web, Eur. J. Mech. A/Solids 25 (2006) 729–744.